View Article Online / Journal Homepage / Table of Contents for this issue

The Symmetrical Octasilasesquioxanes $X_8Si_8O_{12}$: Electronic Structure and Reactivity†

Gion Calzaferri *[,a] **and Roald Hoffmann** *[,b]

[a] *Institute for Inorganic and Physical Chemistry, University of Bern, CH-3000 Bern 9, Switzerland*

[b] *Department of Chemistry and Materials Science Center, Cornell University, Ithaca, NY 14853, USA*

The electronic structure of the octahedral octasilasesquioxanes $X_8Si_8O_{12}$ (X = H, Cl or CH_3) has been analysed in detail and the Si–X stretching mode investigated. It is amazing that among the many orbitals of $H_8Si_8O_{12}$ there is exactly one of A_{2g} symmetry. This pure oxygen lone-pair orbital turns out to be the highest occupied, followed by a number of oxygen lone pairs which interact very slightly with the Si and X atoms. The calculated first ionization energy of 10.7 eV is low but is in good agreement with experimental observations. Analysis of the reaction path of the few experimentally observed substitution reactions, Si–X + Y ⟶ Si–Y + X (X = H or Cl; Y = D, Cl, OCH_3, or $OSiMe_3$), on $X_8Si_8O_{12}$, leads to the result that a five-co-ordinate silicon intermediate is involved, followed by concerted rearrangement of angles and bond distances. The reaction mechanism is dictated by the rigid structure of the Si_8O_{12} framework. This does not allow pseudo-rotation or an attack from the back, thus leading to a new reaction path for four-co-ordinate silicon chemistry. Protonation of a bridging oxygen causes a small weakening of the Si–O bond only, in agreement with the stability of these molecules to acids. It is interesting that no adiabatic ground-state path exists to dissociate $(HO)_3Si$–X into $(HO)_3Si$ + X for X = H, while one is expected to exist for X = Cl or CH_3. Such a dissociative path is costly in energy in all cases, hence intermediates such as $X_7Si_8O_{12}$ can be excluded for reactions of these molecules.

Published on 01 January 1991 on http://pubs.rsc.org | doi:10.1039/DT9910000917
Downloaded by Cornell University on 07 December 2012

The stereochemistry of nucleophilic substitution at four-co-ordinated silicon has been discussed in a recent review article by Holmes.[1] One of the conclusions reached is that when the leaving group at a chiral centre is chlorine, inversion of configuration invariably occurs, while substitution of H happens primarily with retention of the configuration. The observation that much of the reaction chemistry of four-co-ordinated silicon is interpretable in terms of reaction mechanisms involving five-co-ordinated species has given rise to some proposed pathways for nucleophilic displacement that complement those in phosphorus chemistry[2a–c] and very recently the first stable representative of an incipient proton-assisted equatorial bond-cleavage intermediate has been characterized.[2d] In view of these results it is remarkable that the first Si–H substitution reaction in octasilasesquioxane $H_8Si_8O_{12}$ (Scheme 1) was reported by Klemperer and co-workers[3] as late as 1985. The first synthesis of $H_8Si_8O_{12}$ was described more than forty years ago[4] and the X-ray structure of the molecule has been known since 1960.[5] A number of $X_8Si_8O_{12}$ molecules have been synthesised[4,6] but only very recently by substitution of H in $H_8Si_8O_{12}$.[3,7,8] Is there a reason behind this large gap in time between the first synthesis of $H_8Si_8O_{12}$ and the first observed substitution reaction on this molecule?

The molecule $H_8Si_8O_{12}$ is fairly stable and can be prepared from dilute-solution hydrolysis of $SiH(OCH_3)_3$ with concentrated hydrochloric acid in a cyclohexane–acetic acid medium, followed by crystallization from cyclohexane as colourless needles or cubes.[6] It melts at 250 °C and can be sublimed at temperatures below 100 °C. While unstable under basic conditions, it is not affected by dilute acids. Its proton NMR and its silicon NMR spectrum each consist of a single line.[6f] To carry out detailed IR and Raman spectroscopic studies on this molecule is very attractive because of the high symmetry.[9] If H is substituted for methyl, the molecule becomes thermally very stable and is not affected by moderate acidic or basic treatments. Substitution of H for Cl results in a molecule which is sensitive towards moisture; $Cl_8Si_8O_{12}$ is, however, less reactive and therefore easier to handle than many other chlorosilanes.[3,10]

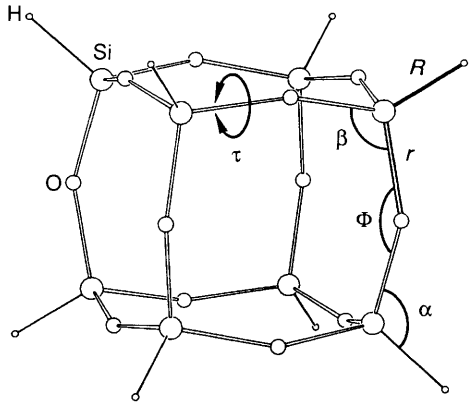

Scheme 1

No Si–X + Y ⟶ Si–Y + X substitution reactions have been reported up to now on $(CH_3)_8Si_8O_{12}$ and its alkyl and aryl analogues, but there is clear evidence that the substitution reactions $X_8Si_8O_{12}$ + 8 Y^- ⟶ $Y_8Si_8O_{12}$ + 8 X^-, summarized in Scheme 2 , can be carried out with good or even with very good yield and it seems likely that $Cl_8Si_8O_{12}$ can be bound covalently without skeleton rupture on a semiconductor surface such as Si, Ge, ZnSe, and others.[10]

Two basically different paths can be imagined by which a substitution reaction with retention of configuration might occur (Scheme 3). The more attractive one (A) keeps the cage intact, while in the second (B) skeleton rupture occurs, which, however, must be fully reversible. Under the reaction conditions

† *Non-SI unit employed:* eV ≈ 1.60 × 10^{-19} J.

View Article Online

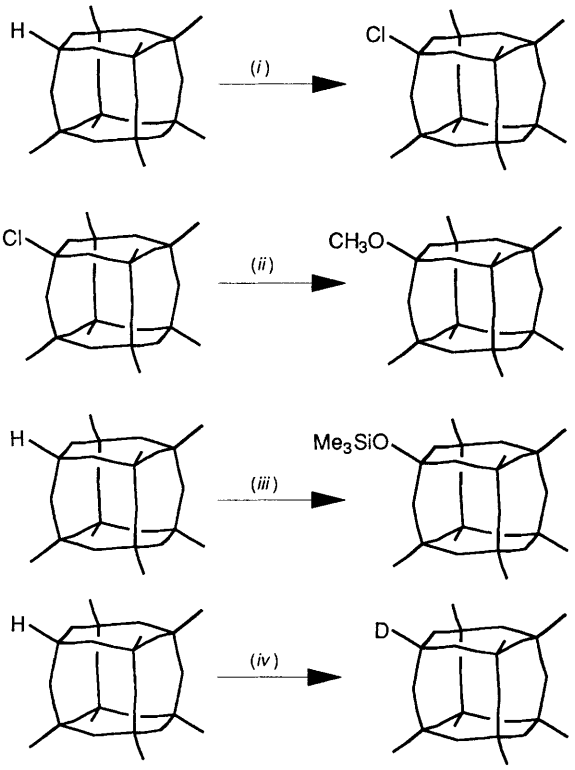

Scheme 2 (*i*) $Cl_2(CCl_4, light)$;[3] (*ii*) CH_3ONO;[3] (*iii*) $Me_3NOSiMe_3Cl$;[7] (*iv*) $D_2(Pd/C)$[8]

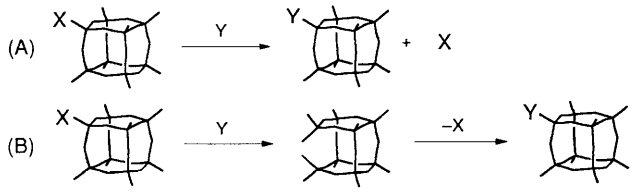

Scheme 3

at which the so far clearly identified reactions occur, skeleton rupture is improbable. Skeleton rupture can happen after interaction of a bridging oxygen with a Lewis acid. We do not intend to discuss it here. It will, however, be interesting to study the influence of protonation of the bridging oxygen on the Si–O bond strength. Protonation of bridging oxygen plays an important role in zeolites. It leads to Brönsted acid sites which are responsible for some of the catalytic properties of zeolites.[11]

In previous studies of the electronic structure of the 4-4 and 6-6 secondary building units, and the β cage, which are typical structures observed in zeolites, high-lying non-bonding oxygen orbitals have been found and some of their consequences have been discussed.[12] This theoretical finding is supported by the valence-band photoelectron spectra of silicon dioxide.[13] Since interaction with Lewis acids and with metal cations depends on the energy of these non-bonding oxygen lone pairs in the highest occupied molecular orbital (HOMO) region, it is interesting to observe that the Si_8O_{12} framework of $H_8Si_8O_{12}$ has close resemblance to the double four-ring D4R found in Linde type A and in CoAPO-50 type zeolites[14] and can therefore be regarded as a test case for calculations on zeolites. This means that detailed insight into the electronic structure of this molecule will also help to improve the understanding of the more complicated zeolites and complement recent theoretical studies on similar systems.[15]

To obtain a transparent description of $X_8Si_8O_{12}$, X = H, Cl, or CH_3, of larger spherosiloxanes, and probably of zeolites, the molecular orbitals (MOs) are built as far as possible from symmetry arguments. It turns out that helpful insight into the electronic structure and reactivity of $X_8Si_8O_{12}$ can be gained by studying the much simpler model compounds $SiX(OH)_3$. We therefore discuss the electronic structure of these molecules and their Si–X stretching reaction coordinate first. After this we will be well prepared to understand the electronic structure of $X_8Si_8O_{12}$ and we shall see to what extent $SiX(OH)_3$ can be used as a model for understanding $X_8Si_8O_{12} + Y \longrightarrow YX_7Si_8O_{12} + X$ substitution reactions.

If not otherwise stated, calculations have been carried out by assuming the experimental bond lengths and bond angles in Table 1.[5,16] Details of the extended-Hückel MO calculation procedure are described in the Appendix.

$SiX(OH)_3$ as a Model for the Si–X Bond

We choose the atomic positions and the coordinate system of this model as shown in Scheme 4. The numbering of the atoms is as follows: 1 = Si; 2,3,4 = O; 5 = X; 6,7,8 = H. The three OH groups are arranged in such a way that C_{3v} symmetry is fully maintained. This allows a most transparent analysis of the orbitals and of the reaction paths to be discussed. As we shall see, it also represents the best possible model for describing the Si–X bond in $X_8Si_8O_{12}$. Bond lengths and bond angles as reported in Table 1 will be used for the calculations on $SiX(OH)_3$.

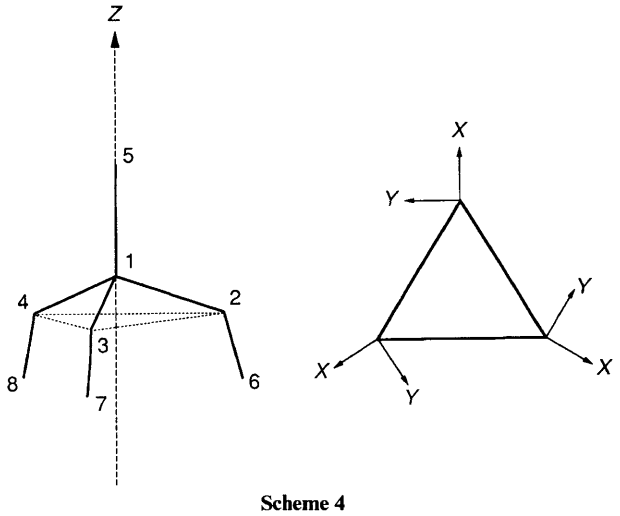

Scheme 4

It is easy to prepare the symmetry-adapted atomic orbitals (AOs) from which we then build the MOs of $SiX(OH)_3$, all of them belonging either to A_1 or the E species with the exception of the p_y oxygen orbitals which belong to A_2 and to E; see Table 2.

The irreducible representations of the MOs of $SiX(OH)_3$ are in equations (1)–(3). The resulting MOs are quite simple

$$\Gamma_{MO}(X = H) = 7A_1 + A_2 + 6E \quad (1)$$

$$\Gamma_{MO}(X = Cl) = \Gamma_{MO}(X = H) + A_1 + E \quad (2)$$

$$\Gamma_{MO}(X = CH_3) = \Gamma_{MO}(X = H) + 2A_1 + 2E \quad (3)$$

enough, so that we may write them explicitly. We proceed in three steps, starting with the construction of the MOs of the SiO_3 fragment, then studying what happens if the free oxygen valences are saturated by three H atoms, and finally exploring the reaction path $(HO)_3Si + H \longrightarrow (HO)_3Si–H$.

We build the molecular orbitals of $O_3Si–X$ as a linear combination of the two fragments O_3 and Si, neglecting in a first step the three H atoms co-ordinated to the three oxygen atoms. In a ZDO approach, the symmetry-adapted MOs of O_3 can be written as[17] in equations (4)–(6). It is easy to see that the A_2, the

Published on 01 January 1991 on http://pubs.rsc.org | doi:10.1039/DT9910000917
Downloaded by Cornell University on 07 December 2012

View Article Online

$$\Psi_A = 1/\sqrt{3}\,(\varphi_1 + \varphi_2 + \varphi_3) \quad (4)$$

$$\Psi_{E_a} = 1/\sqrt{6}\,(2\varphi_1 - \varphi_2 - \varphi_3) \quad (5)$$

$$\Psi_{E_b} = 1/\sqrt{2}\,(\varphi_2 - \varphi_3) \quad (6)$$

five A_1, and the four E orbitals of SiO_3 can be written as in equations (7)–(10) where N is a mixing and normalization coefficient.

$$\Psi(A_2) = N_{A_2}/\sqrt{3}(2p_{y_2} + 2p_{y_3} + 2p_{y_4}) \quad (7)$$

$$\begin{aligned}\Psi_j(nA_1) = {} & N_{(2s)j}/\sqrt{3}(2s_2 + 2s_3 + 2s_4) \\ & + N_{(2p_{z_3})j}/\sqrt{3}(2p_{z_2} + 2p_{z_3} + 2p_{z_4}) \\ & + N_{(2p_x)j}/\sqrt{3}(2p_{x_2} + 2p_{x_3} + 2p_{x_4}) \\ & + d_j{\cdot}3p_{z_1} + a_j{\cdot}3s_3 \end{aligned} \quad (8)$$

$$\begin{aligned}\Psi_j(E_a) = {} & N_{(2s)j}/\sqrt{6}(2{\cdot}2s_2 - 2s_3 - 2s_4) \\ & + N_{(2p_z)j}/\sqrt{6}(2{\cdot}2p_{z_2} - 2p_{z_3} - 2p_{z_4}) \\ & + N_{(2p_x)j}/\sqrt{6}(2{\cdot}2p_{x_2} - 2p_{x_3} - 2p_{x_4}) \\ & + N_{(2p_y)j}/\sqrt{2}(2p_{y_3} - 2p_{y_4}) + b_j{\cdot}3p_{x_1} \end{aligned} \quad (9)$$

$$\begin{aligned}\Psi_j(E_b) = {} & N_{(2s)j}/\sqrt{2}(2s_3 - 2s_4) \\ & + N_{(2p_z)j}/\sqrt{2}(2p_{z_3} - 2p_{z_4}) \\ & + N_{(2p_x)j}/\sqrt{2}(2p_{x_3} - 2p_{x_4}) \\ & + N_{(2p_y)j}/\sqrt{6}(2{\cdot}2p_{y_2} - 2p_{y_3} - 2p_{y_4}) + c_j{\cdot}3p_{y_1} \end{aligned} \quad (10)$$

Table 1 Bond lengths (Å) and angles (°) of $H_8Si_8O_{12}$[5,16]

Coordinate		Coordinate	
R(Si–H)	1.45	α(O–Si–H)	109.5
r(Si–O)	1.62	β(O–Si–O)	109.5
		Φ(Si–O–Si)	147.7

Table 2 AOs to build the $SiX(OH)_3$ MOs; C_{3v} symmetry

X		Si		3O		3H	
ns	A_1	3s	A_1	2s	A_1,E	1s	A_1,E
np_z	A_1	$3p_z$	A_1	$2p_z$	A_1,E		
(np_x,np_y)	E	$(3p_x,3p_y)$	E	$2p_x$	A_1,E		
				$2p_y$	A_2,E		

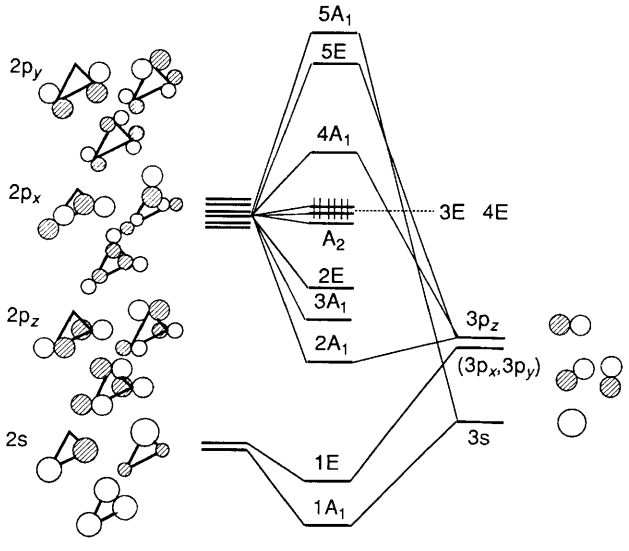

Fig. 1 Correlation diagram for 3O + Si → SiO_3; C_{3v} symmetry. The two-fold degenerate 3E plus 4E orbitals are occupied by six electrons

Obviously, A_2 is a pure oxygen lone-pair orbital and the A_1 orbitals are fully responsible for the interaction of the hydrogen atom with the silicon. The large energy difference between the oxygen 2p and 2s orbitals and between the silicon 3s and 3p orbitals leads to well distinguished energy levels even if they belong to the same irreducible representation. This can be understood from second-order perturbation theory which leads to the general result that the magnitude of interaction between two levels is inversely proportional to the energy difference between them.[18] As a consequence of the local D_{3h} symmetry of the O_3 fragment, the E($2p_y$) orbitals form a set of lone pairs, disturbed only by oxygen E($2p_x$) and oxygen E($2p_z$) orbitals. This is clearly reflected in the results collected in Table 3, where the calculated coefficients and the corresponding energies are gathered.

The $1A_1$ and the ($1E_a$,$1E_b$) orbitals correspond to nearly pure σ(2s + 3s) bonds while the ($4E_a$,$4E_b$) and ($3E_a$,$3E_b$) orbitals are due to oxygen lone pairs. This finding, which is based on the symmetry of the system and on the energy difference between the s and the p orbitals, is illustrated in Fig. 1, where we show on the left side the symmetry-adapted linear combination of the oxygen AOs, on the right side the Si AOs, and in the middle the MOs of SiO_3.

To develop a more realistic model for describing the O_3Si–H fragment in $H_8Si_8O_{12}$, the free oxygen valences of the O_3Si model compound must be saturated by binding H atoms to them. This means that the A_1 and the E combination of three 1s(H) orbitals will interact with the appropriate MOs of SiO_3. From the data in Table 3 it is obvious that the bonding interaction will take place with the $2A_1$ and the 2E orbitals. It is not astonishing that the $4A_1$ orbital is also stabilized; see Fig. 2. We notice that the 3E and the 4E orbitals are slightly stabilized and move below the A_2 oxygen lone pair. This is interesting because we shall encounter the same situation in the $H_8Si_8O_{12}$ molecule. Such an orbital should easily be detectable in a photoelectron spectrum because, as a consequence of its pure lone-pair character, Koopmans' theorem is expected to be well satisfied.[19,20] We shall come back to this in the next section. Note that at this point we have reached a molecular structure, $(HO)_3Si$, which a chemist would write as a simple radical, placing the odd electron in an orbital directed away from the Si (Scheme 5). The MO corresponding to that radical lobe is $4A_1$.

We are now ready to investigate what happens if H and $(HO)_3Si$ are brought together along the reaction coordinate illustrated in Scheme 6. The only orbitals involved in such a reaction are those of A_1, symmetry, which makes the discussion

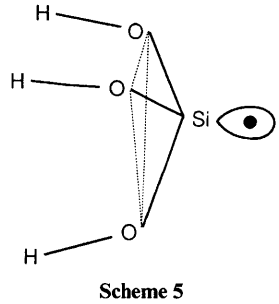

Scheme 5

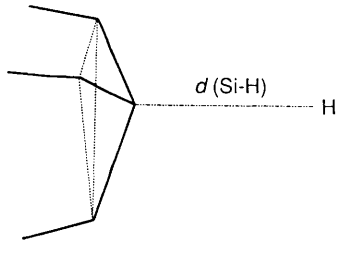

Scheme 6

Published on 01 January 1991 on http://pubs.rsc.org | doi:10.1039/DT9910000917
Downloaded by Cornell University on 07 December 2012

View Article Online

Table 3 Calculated coefficients and energies of the orbitals given in equations (7)–(10)

Γ_{MO}	$N_{2s}/\sqrt{3}$		$N_{2p_z}/\sqrt{3}$		$N_{2p_x}/\sqrt{3}$		$N_{2p_y}/\sqrt{3}$		$d(3p_z)$	$a(3s)$	ε_i/eV
A_2							0.58				−10.75
$5A_1$	0.50				−0.42				−0.59	−1.02	13.95
$4A_1$	0.50		0.54						−0.54	0.22	−9.00
$3A_1$	−0.17		−0.42		−0.42				0.42	0.09	−12.67
$2A_1$	0.20		0.59		0.59				0.59	−0.49	−15.36
$1A_1$	0.40									0.45	−30.88

Γ_{MO}	$N_{2s}/\sqrt{6}$	$N_{2s}/\sqrt{2}$	$N_{2p_z}/\sqrt{6}$	$N_{2p_z}/\sqrt{2}$	$N_{2p_x}/\sqrt{6}$	$N_{2p_x}/\sqrt{2}$	$N_{2p_y}/\sqrt{6}$	$N_{2p_y}/\sqrt{2}$	$b(3p_x)$	$c(3p_y)$	ε_i/eV
$5E_a\ 5E_b$	0.30	0.51	0.21	−0.28	−0.28	0.25	0.12	−0.2	1.14	1.14	6.60
$4E_a\ 4E_b$			−0.25			0.26	0.18	−0.3			−10.74
$3E_a\ 3E_b$					0.24	−0.34	0.56	−0.34			−10.81
$2E_a\ 2E_b$	−0.11	−0.18	−0.27	0.38	0.38	0.16	−0.15	0.16	0.29	0.29	−12.03
$1E_a\ 1E_b$	0.34	0.6							0.29	−0.29	−27.82

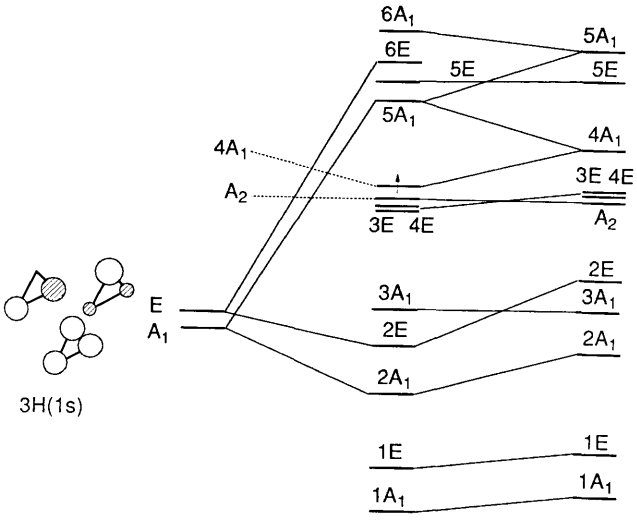

Fig. 2 Correlation diagram for $3H + O_3Si \rightarrow (HO)_3Si$. The $4A_1$ orbital of $(HO)_3Si$ is occupied by one electron

simple. It can be further simplified by dropping the very low and the very high lying orbitals, which are not much involved in the bonding. This leads to the correlation diagram presented in Fig. 3. The four-orbital interaction between 1s on H and $2A_1$, $3A_1$, and $4A_1$ on $(HO)_3Si$ sorts itself out in such a way that most of the Si–H bonding is in '$2A_1$', the antibonding in '$4A_1$'. The hydrogen character is distributed over all the A orbitals. The interaction with the $3A_1$ level leads to an orbital we call A_1(1s-H) for reasons easily understood by inspection of the right-hand side of Fig. 3. Stabilization and destabilization of $3A_1$ are approximately equal. As a consequence, this interaction does not contribute much to the Si–H bond strength.

If, however, we would like to understand what happens along the reaction path in Scheme 6, the behaviour of the A_1(1s-H) orbital must be investigated. In Fig.4 we show the calculated potential-energy curve for $SiH(OH)_3$ from which it follows that a dissociative pathway would cost far too much energy to explain reaction (11). The experimental Si–H bond strength is of

$$H_8Si_8O_{12} + 4D_2 \rightarrow D_8Si_8O_{12} + 4H_2 \qquad (11)$$

the order of 4 eV. An intermediate such as $H_7Si_8O_{12}$ cannot therefore be investigated to explain the deuterium-exchange reaction [8] and we have to search for an alternative.

The energy needed to break the Si–H bond is due to the increase of the $2A_1$ orbital energy. A correct description of the reaction path is, however, more involved. We will come back to this soon. First Fig. 4 must be explained in more detail. The dotted curve represents the extended-Hückel binding energy $\Delta E_{EHMO}(R)$ as function of the bond distance R. The 'repulsive' dashed curve is the electrostatic two-body correction $E_{\alpha\beta}(R)$ and the solid curve $E(R)$ is the sum in equation (12). It describes

$$E(R) = E_{\alpha\beta}(R) + \Delta E_{EHMO} \qquad (12)$$

the potential of the Si–H stretching mode, see also Appendix. We are using a slight modification of Anderson's ASED-MO method.[21,22] The procedure is designed to repair the deficiencies of the extended-Hückel method in calculating bond distances; note for instance the lack of a minimum in the extended-Hückel energy (dotted line) in Fig. 4.

Let us look at the correlation diagram in Fig. 5, to explain what happens. Stretching the Si–H bond causes an increase in energy of the $2A_1$ and of the A_1(1s-H) orbitals, while the $3A_1$ and especially the $4A_1$ orbitals are stabilized. This simple description is reasonable until we reach a certain bond distance, somewhere between 2.5 and 3.5 Å, indicated by a vertical arrow in Fig. 5, where a dramatic event will occur, unless provisions are taken. In this region the A_1(1s-H) level is gradually growing into a nearly pure 1s(H) orbital filled by two electrons. This corresponds to the situation of weakly interacting $(HO)_3Si^+ + H^-$ ions. Such an ion pair would, however, have much higher energy than the neutral fragments $(HO)_3Si + H$. The ionization energy of H^- is approximately 0.75 eV. This means that the energy of the ion pair is $-\{\varepsilon[4A_1, d(Si–H) = \infty] - 0.75\} \sim 9.5$ eV larger than that of the radical pair. We conclude that no adiabatic ground-state path exists to dissociate $SiH(OH)_3$ into $(HO)_3Si + H$.

We describe the same reaction path again, now by approaching H towards $(HO)_3Si$ from infinity. In this initial state, the $4A_1$ orbital of $(HO)_3Si$ is occupied by one electron (right-hand side of Fig. 5) and the A_1(1s-H) orbital is also occupied by one electron. If we approach the two molecular pieces slowly, the excited-state electron configuration $[A_1(1s\text{-}H)]^1(4A_1)^1$ will result. To stabilize the situation, a spontaneous $A_1(1s\text{-}H) \leftarrow (4A_1)$ transition must occur. This electronic transition is allowed. Depending on the conditions, a reaction of this kind could be accompanied by intense luminescence. The situation we observe here is reminiscent of the well understood reactions of ionic dimers and the so-called harpoon mechanism observed in reactions as *e.g.* $Br_2 + K \rightarrow KBr_2^* \rightarrow KBr + Br$.[23] The first stage in this reaction is envisaged as the transfer of the valence electron of the alkali-metal atom to the halogen molecule. Such a transfer is possible even when reactants are quite a few angströms apart. Basically one has a composite molecular ground state that correlates to an ionic excited state of separated atoms (Fig. 6, left). This leads to a problem for the calculation of the potential-energy curve of $SiH(OH)_3$ for larger Si–H distances than shown in Fig. 4. Crossing between the two curves corresponding to electron configurations $\{[A_1(1s\text{-}H)]^2(4A_1)^0\}$ and $\{[A_1(1s\text{-}H)]^1(4A_1)^1\}$ will occur somewhere along the reaction coordinate.

Published on 01 January 1991 on http://pubs.rsc.org | doi:10.1039/DT9910000917
Downloaded by Cornell University on 07 December 2012

View Article Online

Downloaded by Cornell University on 07 December 2012
Published on 01 January 1991 on http://pubs.rsc.org | doi:10.1039/DT9910000917

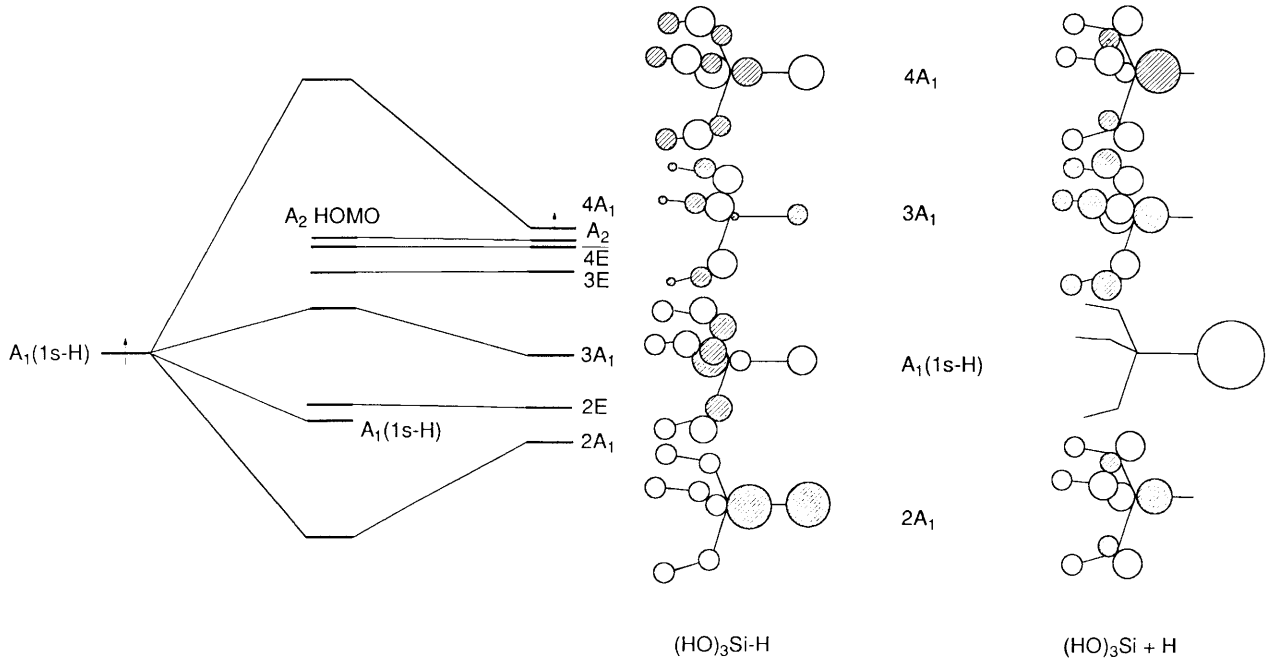

Fig. 3 Orbital energies along the path in Scheme 6. On the right-hand side are shown the wave-functions of A_1 symmetry: left $(HO)_3Si–H$ and right $(HO)_3Si + H$

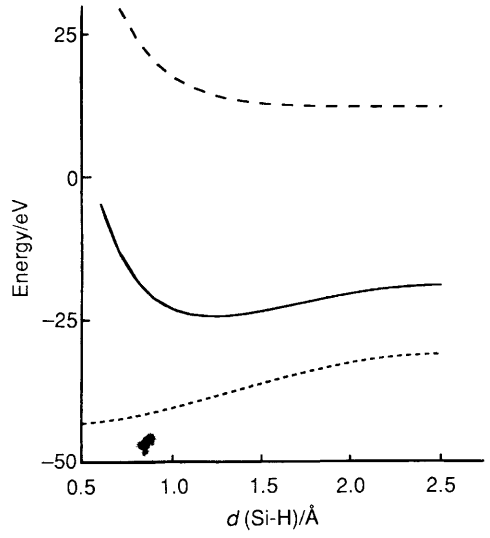

Fig. 4 The Si–H stretching mode of $SiH(OH)_3$. (------) Two-body interaction $E_{\alpha\beta}(R)$, (• • • •) $\Delta E_{EHMO}(R)$, (——) $\Delta E_{EHMO}(R) + E_{\alpha\beta}(R)$

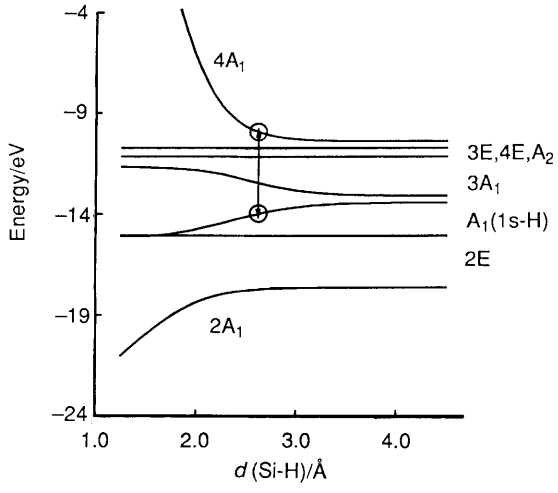

Fig. 5 Correlation diagram along the Si–H path in Scheme 6. Left: $SiH(OH)_3$ at equilibrium bond distance, the LUMO is $4A_1$. Right: $(OH)_3Si + H$, the $4A_1$ and the A_1(1s-H) orbitals are filled with one electron each

What changes for $SiCl(OH)_3$? We are not astonished to find that the Si–Cl interaction is dominated by orbitals of A_1 symmetry which describe the sigma bond, as shown in Fig. 7 Two significant differences between Fig. 3 and this figure can be observed. The $3p_z$ of the Cl is involved in the bonding. More important, the $4A_1$ orbital and 3p orbitals in the separated fragments are at approximately the same energy. This means that we expect potential-energy curves as depicted on the right-hand side of Fig. 6. Hence, it should be possible to calculate the potential from a simple bond elongation in this case. The result is shown in Fig. 8. A photochemical dissociative pathway involving the $4A_1 \leftarrow E$(p-Cl) electronic transition is unlikely, given the large energy difference of about 14 eV between the $4A_1$ and the E(p-Cl) levels.

A new interaction can be observed in $SiCH_3(OH)_3$ relative to $SiCl(OH)_3$. While the Si–H and the Si–Cl potential-energy curves depend crucially on the two-body interaction term $E_{\alpha\beta}(R)$,[21,22] reliable Si–C bond lengths can be obtained by the EHMO method without this repulsive term. Why is this so? In Fig. 9 we show the Si–CH_3 potential. It is obvious that

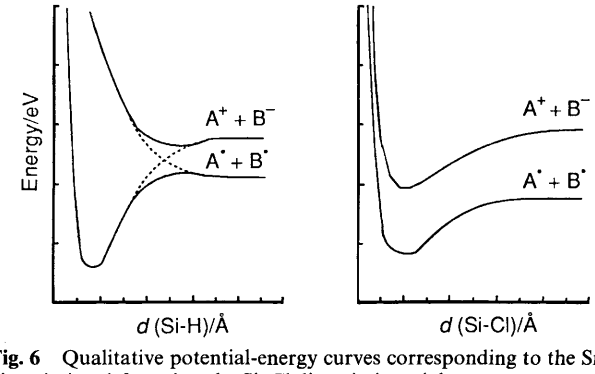

Fig. 6 Qualitative potential-energy curves corresponding to the Si–H dissociation, left, and to the Si–Cl dissociation, right

$\Delta E_{EHMO}(R)$ has a well distinguished minimum. It is possible to choose the AOs so that the correct bond lengths are obtained without adding a repulsive term. While small changes in the

View Article Online

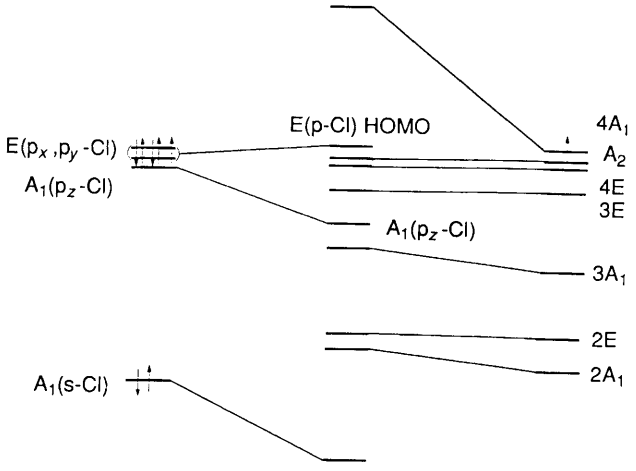

Fig. 7 Correlation diagram for $(HO)_3Si + Cl \rightarrow (HO)_3Si–Cl$

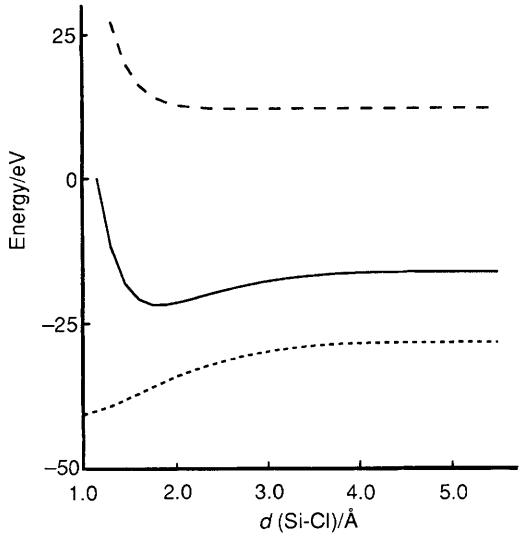

Fig. 8 The Si–Cl stretching coordinate of $SiCl(OH)_3$. See also Fig. 4

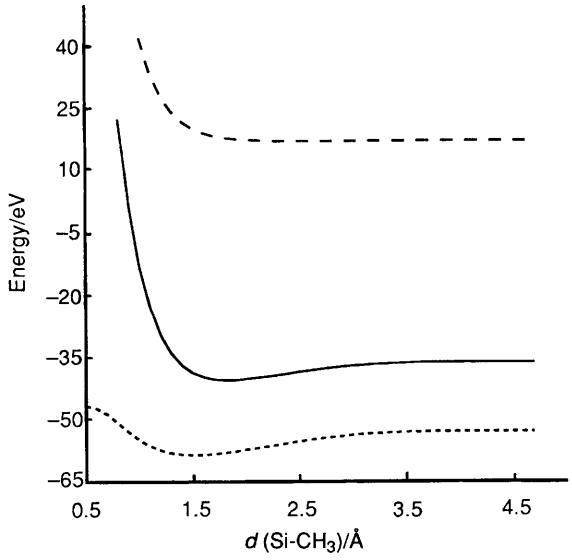

Fig. 9 Potential-energy curve for $SiCH_3(OH)_3$. See also Fig. 4

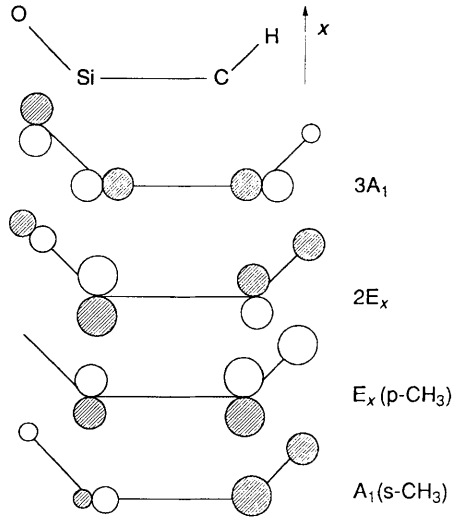

Scheme 7

Slater exponent of Si affect the potential energy, they do not affect the general behaviour of the orbitals. Similar as in the Cl case, the A(s-CH_3) is largely responsible for the Si–CH_3 interaction. However, now also the $3A_1$ orbital comes in. First it goes down, but then becomes repulsive at short bond distances where it suddenly has to change its behaviour to avoid crossing with the $A_1(p_z\text{-}CH_3)$ orbital. The behaviour of these two orbitals is largely responsible for the increase in energy of $\Delta E_{EHMO}(R)$ at short Si–C distances.

Another new feature is that the two-fold degenerate E(p-CH_3) and 2E MOs are no longer inactive. There is nothing new about this interaction, which is hyperconjugation. The molecular orbital representation of hyperconjugation was introduced by Mulliken in 1939[24] and has since been discussed in many different aspects.[25] How hyperconjugation comes in is illustrated in Scheme 7, where we illustrate molecular orbitals of $SiCH_3(OH)_3$ in the O–Si–C–H plane that show significant changes along the Si–C stretching coordinate. Similar to the case of $SiCl(OH)_3$, the $4A_1$ orbital and the $A_1(p_z\text{-}CH_3)$ orbital in the separated fragments are at approximately the same energy. This means again that we expect a potential-energy curve as depicted on the right-hand side of Fig. 6. Hence, it can be calculated for any bond distance without complications. To conclude this section, note that the Si–OH stretching mode of $(HO)_3Si–OH$, not illustrated here, is similar to that observed in Si–Cl.

The Si–X bond strength cannot be the reason for the very different reactivities of $H_8Si_8O_{12}$, $Cl_8Si_8O_{12}$, and $(CH_3)_8Si_8O_{12}$. This is consistent with chemical intuition. In order to explain the different properties of these molecules other arguments have to be considered, some of which have been discussed in this section.

Molecular Orbitals of $X_8Si_8O_{12}$

It is now time to look at the orbitals of the $X_8Si_8O_{12}$ molecules. To do this, we use the numbering and the coordinate system in Scheme 8. It has to be understood in the sense that each Si, each O, and each X are the origin of a local coordinate system such that local C_{4v} symmetry is maintained. This means that all the z axes point in the same direction. These coordinates remain useful when a $X_8Si_8O_{12}$ molecule is brought onto an idealized surface, because C_{4v} symmetry is maintained. The numbering of the atoms is: 1–8 = Si, 9–20 = O and 21–28 = X (X = H, Cl, CH_3, or OH). The edges of the coordinate system correspond for example to the Si atom positions 1–4. Considering the O_h symmetry of $X_8Si_8O_{12}$, it is natural to divide its AOs in three groups, namely the O_{12}, the Si_8, and the X_8. This leads to the irreducible representations in Table 4. We would like to add that the shortest O ··· O and the shortest Si ··· Si distances are 2.64 and 3.11 Å respectively.

It is amazing that among all these orbitals there is exactly one

Published on 01 January 1991 on http://pubs.rsc.org | doi:10.1039/DT9910000917
Downloaded by Cornell University on 07 December 2012

View Article Online

of A_{2g} symmetry, and it is evident that this orbital is due to a pure oxygen lone pair. Because of its very special character it should be the ideal orbital to determine the energy of the oxygen lone-pair electrons. The relevance of this has been mentioned in the Introduction. Remember that in the previous section, Table 3, we have found that A_2 represents a pure oxygen lone pair of $SiX(OH)_3$. The $\Psi_{A_{2g}}$ orbital is of similar character and can be written easily [equation (13)]. Its form is illustrated in Scheme 9

$$\Psi_{A_{2g}} = 1/\sqrt{20}[(p_{y_9} + p_{z_9} + p_{y_{15}} + p_{z_{15}} - p_{y_{11}} - p_{z_{11}} - p_{y_{13}} - p_{z_{13}}) + (-p_{y_{10}} - p_{z_{10}} - p_{y_{16}} - p_{z_{16}} + p_{y_{12}} + p_{z_{12}} + p_{y_{14}} + p_{z_{14}}) + (-p_{x_{17}} - p_{y_{17}} - p_{x_{19}} - p_{y_{19}} + p_{x_{18}} + p_{y_{18}} + p_{x_{20}} + p_{y_{20}})] \quad (13)$$

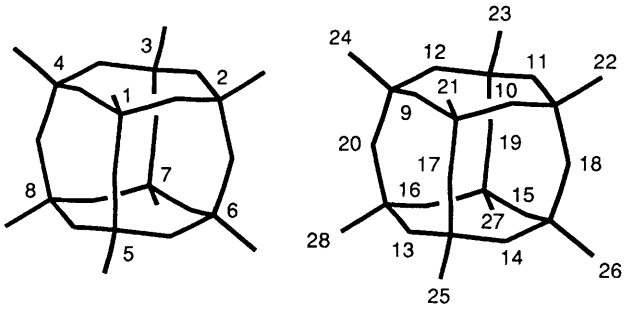

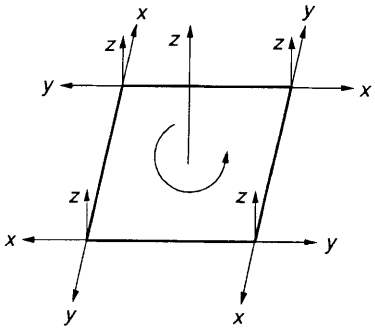

Scheme 8

in one of the three planes containing the oxygen atoms {9,11,15,13}, {10,12,16,14}, and {17,18,19,20}.

Another important set of orbitals that can readily be written down are those belonging to the irreducible representations of $\Gamma_X(s)$ and $\Gamma_{Si}(s)$. We write them for the Si atoms {1,2,3,4,5,6,7,8} [equations (14)–(21)]. For X we only have to change the numbering into {21,22,23,24,25,26,27,28}. Exactly the same linear combinations hold for those Si p AOs which are important in Si–X σ bonding, if we group them first into the sets

Table 4 Irreducible representations of $X_8Si_8O_{12}$ MOs

$\Gamma_O(s) = A_{1g}$		E_g		T_{2g}		T_{1u}	T_{2u}
$\Gamma_O(p) = A_{1g}$	A_{2g}	$2E_g$	$2T_{1g}$	$2T_{2g}$	A_{2u} E_u	$3T_{1u}$	$2T_{2u}$
$\Gamma_{Si}(s) = A_{1g}$				T_{2g}	A_{2u}	T_{1u}	
$\Gamma_{Si}(p) = A_{1g}$		E_g	T_{1g}	$2T_{2g}$	A_{2u} E_u	$2T_{1u}$	T_{2u}
$\Gamma_X(s) = A_{1g}$				T_{2g}	A_{2u}	T_{1u}	
$\Gamma_X(p) = A_{1g}$		E_g	T_{1g}	$2T_{2g}$	A_{2u} E_u	$2T_{1u}$	T_{2u}

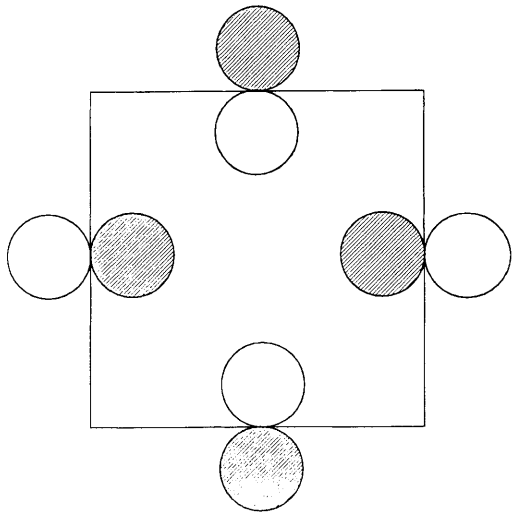

Scheme 9

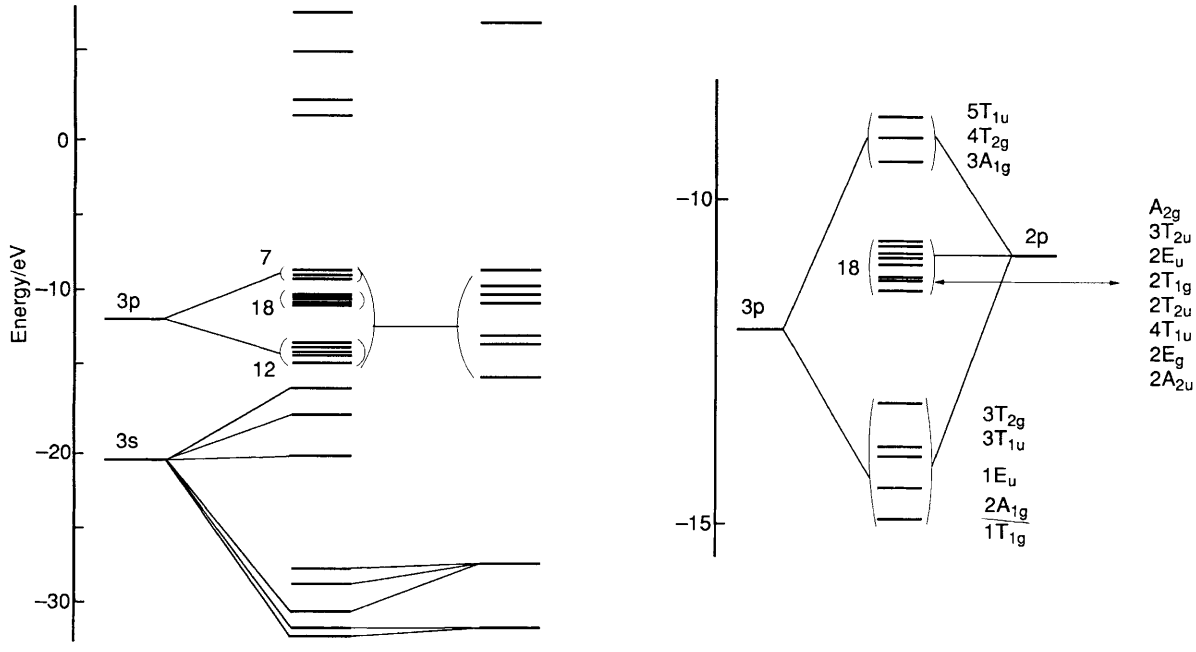

Fig. 10 Correlation diagram. The numbers indicate the number of levels in the corresponding region. Left: 4 Si + 4 $SiO_3 \rightarrow Si_8O_{12}$. Right: the region between −15 and −9 eV magnified. Correlation with the 3p AOs of Si and the 2p AOs of O is shown

Published on 01 January 1991 on http://pubs.rsc.org | doi:10.1039/DT9910000917
Downloaded by Cornell University on 07 December 2012

View Article Online

$$\Psi^{s}_{A_{1g}} = 1/\sqrt{8}(s_1 + s_2 + s_3 + s_4 + s_5 + s_6 + s_7 + s_8) \quad (14)$$

$$\Psi^{s}_{A_{2u}} = 1/\sqrt{8}(s_1 - s_2 + s_3 - s_4 - s_5 + s_6 - s_7 + s_8) \quad (15)$$

$$\Psi^{s}_{T_{2g}}(a) = 1/\sqrt{8}(s_1 - s_2 + s_3 - s_4 + s_5 - s_6 + s_7 - s_8) \quad (16)$$

$$\Psi^{s}_{T_{2g}}(b) = 1/\sqrt{8}(-s_1 - s_2 + s_3 + s_4 + s_5 + s_6 - s_7 - s_8) \quad (17)$$

$$\Psi^{s}_{T_{2g}}(c) = 1/\sqrt{8}(s_1 - s_2 - s_3 + s_4 - s_5 + s_6 + s_7 - s_8) \quad (18)$$

$$\Psi^{s}_{T_{1u}}(a) = 1/\sqrt{8}(s_1 + s_2 + s_3 + s_4 - s_5 - s_6 - s_7 - s_8) \quad (19)$$

$$\Psi^{s}_{T_{1u}}(b) = 1/\sqrt{8}(s_1 + s_2 - s_3 - s_4 + s_5 + s_6 - s_7 - s_8) \quad (20)$$

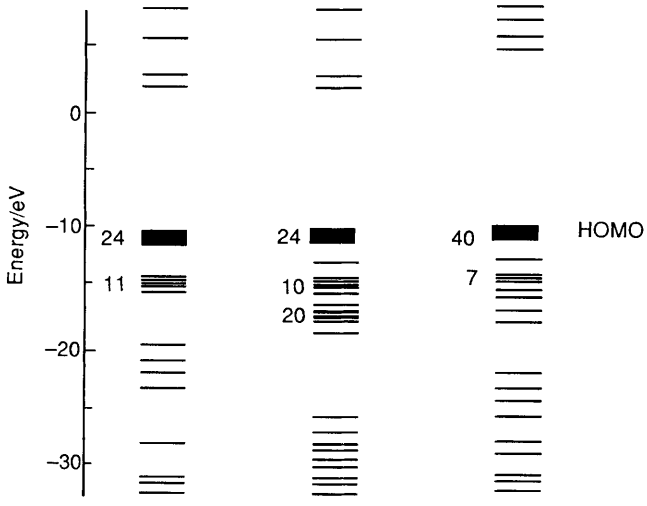

Fig. 11 MO level diagram. From left to right: $H_8Si_8O_{12}$, $(CH_3)_8Si_8O_{12}$, and $Cl_8Si_8O_{12}$. The numbers indicate the number of levels in the corresponding region

$$\Psi^{s}_{T_{1u}}(c) = 1/\sqrt{8}(s_1 - s_2 - s_3 + s_4 + s_5 - s_6 - s_7 + s_8) \quad (21)$$

$1/\sqrt{3}(p_x + p_y + p_z)$ for {1,2,3,4} and $1/\sqrt{3}(p_x + p_y - p_z)$ for {5,6,7,8}.

We now know all the orbitals required to build the Si–X sigma bonds. They have the same general character as those found in $(HO)_3Si$, Fig. 2. As in the previous section, we first build the orbitals of Si_8O_{12} and then we discuss the $X_8Si_8O_{12}$ molecule by adding 8X ligands to this fragment. The local symmetry of each of the SiO_3 fragments in Si_8O_{12} is C_{3v}. We already know the orbitals of SiO_3. It therefore seems interesting to find out what changes occur if we go from 4 SiO_3 + 4 Si to Si_8O_{12}. The correlation diagram in Fig. 10 shows that the state density in the HOMO region increases in Si_8O_{12} with respect to SiO_3 and that levels are built which originate from antibonding or non-bonding interactions of Si with the oxygen of SiO_3. No dramatic changes are observed, which means that an important part of the electronic structure of Si_8O_{12} is prebuilt in the SiO_3 fragment, see also Fig. 2.

The HOMO region between −15 and −9 eV is magnified on the right-hand side of Fig. 10. It is interesting that the A_{2g}, equation (13) and Scheme 9, is the highest-lying orbital of the group of 18 oxygen lone pairs. The $3A_{1g}$, $4T_{2g}$, and $5T_{1u}$ orbitals, whose form is given in equations (14)–(21), are occupied by six electrons, leaving room for 8 X to bind to the 8 Si. These orbitals have the same symmetry as that of the s orbitals of X and are therefore involved in the Si–X bonding of $X_8Si_8O_{12}$. The Si–X bonding mechanism is the same as discussed for $SiX(OH)_3$

At this point it is interesting to discuss the one-electron levels of $H_8Si_8O_{12}$, of $(CH_3)_8Si_8O_{12}$, and of $Cl_8Si_8O_{12}$ in Fig. 11. We first note that the HOMO region starts at about −10.7 eV in $H_8Si_8O_{12}$ and at slightly higher energy in the other cases and that the energy gap between the HOMO and the lowest unoccupied molecular orbital (LUMO) is of the order of 12–14 eV. To get a feeling for the consequences of this relatively high-lying HOMO, we compare it with the first ionization energy of water, observed at 12.6 eV and attributed to the energy of the p-type oxygen lone pair of the water molecule.[20] The simplest of the $X_8Si_8O_{12}$ molecules is $H_8Si_8O_{12}$. In this molecule the HOMO is the $\Psi_{A_{2g}}$ orbital as shown in Fig. 12. Due to its

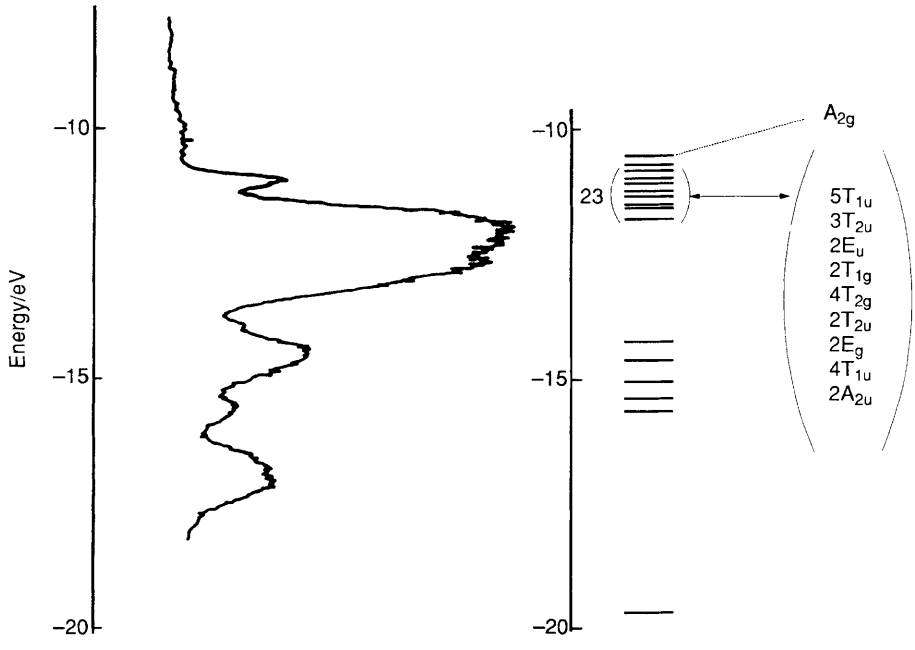

Fig. 12 Photelecton spectrum of $H_8Si_8O_{12}$[26] (left) and calculated one-electron levels (right)

Published on 01 January 1991 on http://pubs.rsc.org | doi:10.1039/DT9910000917
Downloaded by Cornell University on 07 December 2012

View Article Online

Published on 01 January 1991 on http://pubs.rsc.org | doi:10.1039/DT9910000917
Downloaded by Cornell University on 07 December 2012

symmetry it cannot interact with AOs from other centres than oxygen. It is closely followed by a number of levels in the region between −10.75 and −11.7 eV, all of them bearing oxygen lone-pair character but slightly perturbed by interactions with the Si or the H atoms. The next orbitals, found in the region between −14 and −16 eV, have some Si–O bonding character. There is close similarity to the energy levels found in the 4-4 secondary building unit of zeolites, for which some of the consequences of the high-lying oxygen lone pairs have been discussed.[12] The low first ionization energy of 10.7 eV is in good agreement with valence-band photoelectron spectra of silicon dioxide[13] and with recent self consistent field (SCF)-MO calculations on $(HO)_3Si–O–Si(OH)_3$.[11f] Electronic transitions have been reported to occur with photons of energies higher than 10 eV.[13]

A more direct test of the nature and the energy of the HOMO is possible by comparing the photoelectron spectrum of $H_8Si_8O_{12}$ with the calculated levels, Fig. 12. The photoelectron spectrum starts with a sharp peak, indicating the first ionization energy is at about 10.7 eV, followed by a broad intense band and several smaller bands between 14 and 16 eV.[26] This pattern is well simulated by the calculated energy levels. We propose that the first band corresponds to the ionization of an A_{2g} lone-pair electron and the large band to the ionization of the narrow band of 23 levels below. It seems that the smaller bands between 14 and 17 eV are well represented by the calculated levels in the region of 15 eV. The first transitions can be summarized as in Scheme 10. Let us add that the first band has the typical shape usually found in lone-pair transitions. For a more thorough interpretation of photoelectron spectra of silicon compounds we refer to ref. 27.

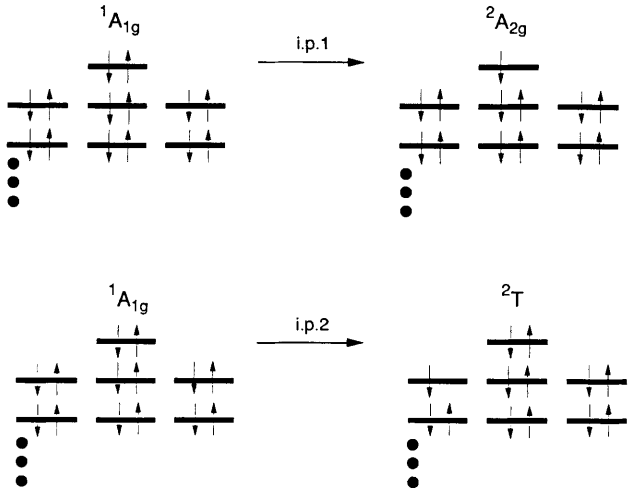

Scheme 10

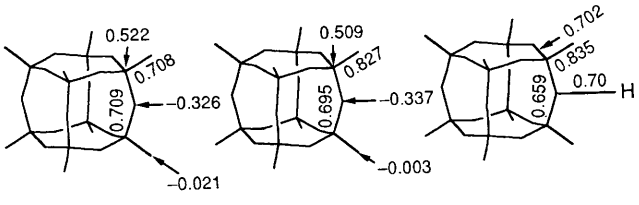

Fig. 13 Overlap population and charge distribution in: $(CH_3)_8Si_8O_{12}$, left; $H_8Si_8O_{12}$, middle; and $[H_9Si_8O_{12}]^+$, right. The numbers without arrows indicate the overlap populations, the others represent charges. For $[H_9Si_8O_{12}]^+$ only overlap populations are shown

In $(CH_3)_8Si_8O_{12}$ and in $Cl_8Si_8O_{12}$ the A_{2g} orbital is no longer so clearly the HOMO. It is buried in a number of 'less pure' oxygen lone pairs. We therefore expect a less structured photoelectron spectrum and the first ionization energy to be somewhat smaller.

The molecule $H_8Si_8O_{12}$ is not very sensitive to dilute acids. One would expect that protonation of at least one of the oxygens occurs readily because of the low ionization energy. From this it follows that protonation of only one of the bridging oxygens should have little effect on the Si–O bond strength. In the extended-Hückel calculation this is reflected in the relatively small decrease of the Si–O overlap population in the protonated molecule with respect to the unprotonated, see Fig. 13. We conclude that protonation of at least two adjacent oxygens is needed to induce skeleton rupture. Under strongly acidic conditions protonation of the Si might also play a role in skeleton rupture of $H_8Si_8O_{12}$, a reaction which is not investigated in this paper. In the last section we observed that hyperconjugation must be considered in the $O_3Si–CH_3$ bonding. Of course, the same is true for $(CH_3)_8Si_8O_{12}$. It influences also the Si–O bond strength in comparison to $H_8Si_8O_{12}$, which is reflected in a small increase of the Si–O overlap population.

Substitution of X

Understanding the electronic structure of the $X_8Si_8O_{12}$ molecules and the Si–X stretching mode, we are well prepared to investigate the pathways of the substitution reactions in Scheme 2. Let us start with the deuterium exchange. We already know that a reaction path involving an intermediate such as $H_7Si_8O_{12}$ can be excluded. We therefore search for another possibility, studying the interaction of the $(HO)_3Si$ model with molecular H_2 along coordinates **I**, **II** and **III** in Scheme 11. These coordinates are sufficient to describe a three-dimensional reaction path in which an H atom approaches Si–H as shown in

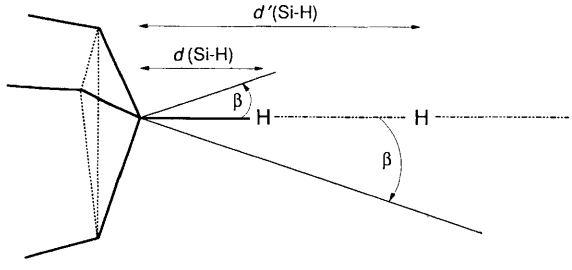

Scheme 12

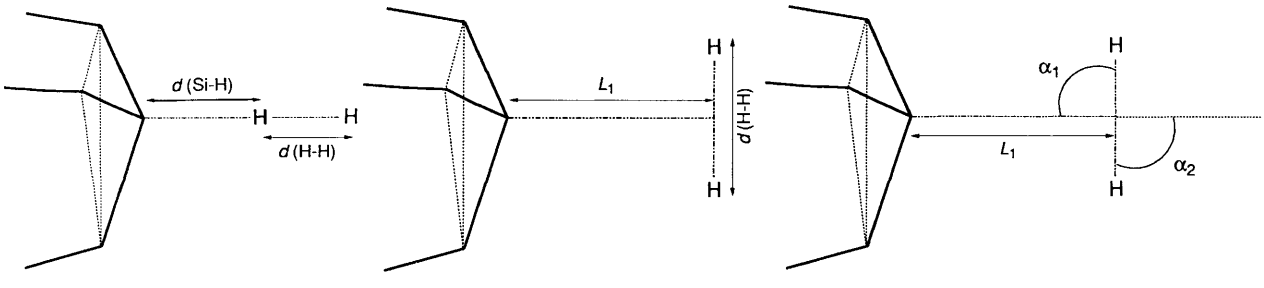

I **II** **III**

Scheme 11

View Article Online

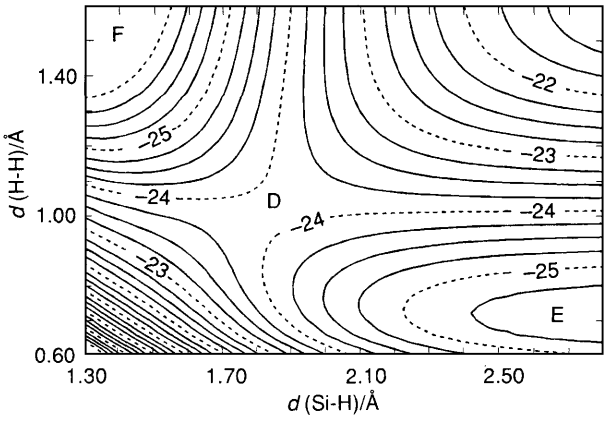

Fig. 14 Potential surface for the apical end-on approach **I**. Energies in eV. The energy separation of two contours is 0.25 eV

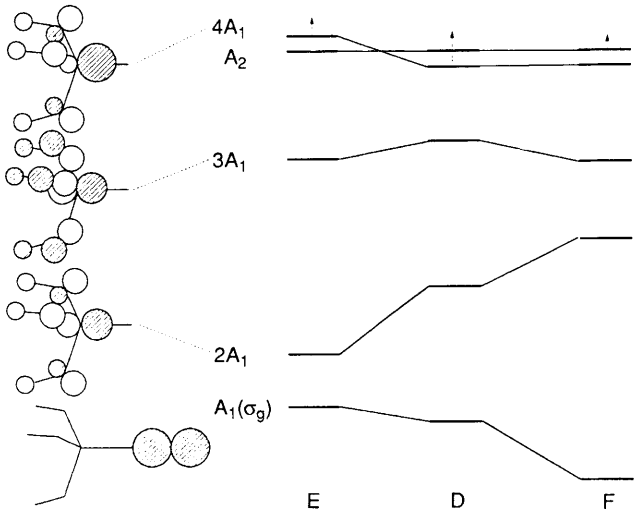

Fig. 15 Correlation diagram along E→D→F in Fig. 14

Scheme 12. The energies calculated with our method are not expected to be very accurate. We believe, however, that they are good enough to investigate the main features of the reaction paths under discussion.

To begin we examine the apical end-on approach **I**, the potential-energy surface of which is shown in Fig. 14. This path alone cannot lead to an exchange reaction, but it is nevertheless interesting to see what happens. Starting at point E, the minumum-energy path leads to the saddle point D at about 1.6 eV higher energy with respect to E, and then falls to the minimum at F. The path E $\rightleftharpoons$ D $\rightleftharpoons$ F corresponds to the reaction (22).

$$(HO)_3Si + H_2 \rightleftharpoons (HO)_3Si \cdots H \cdots H \rightleftharpoons (HO)_3Si\text{–}H + H \quad (22)$$

It is not difficult to guess the origin of the saddle point which has to be crossed. It must be connected with the energy needed to break the Si–H bond if we approach it from F or to break the H–H bond if we approach D from E. The energy needed to cross the barrier is, however, much smaller than the corresponding dissociation energy. Why is this so? The question can be answered by looking at the correlation diagram in Fig. 15. Since only orbitals of A_1 symmetry are involved in the Si–H bond, the wavefunctions along the reaction path **I** can be written as in equation (23) where $A_1(\sigma_g)$ and iA_1 denote the corresponding

$$\Psi_I = a_{I1}A_1(\sigma_g) + \sum_{i=1}^{4} c_{Ii}(iA_1) \quad (23)$$

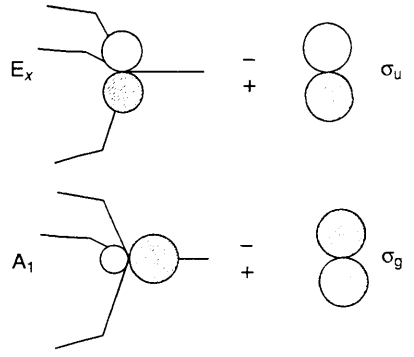

Scheme 13

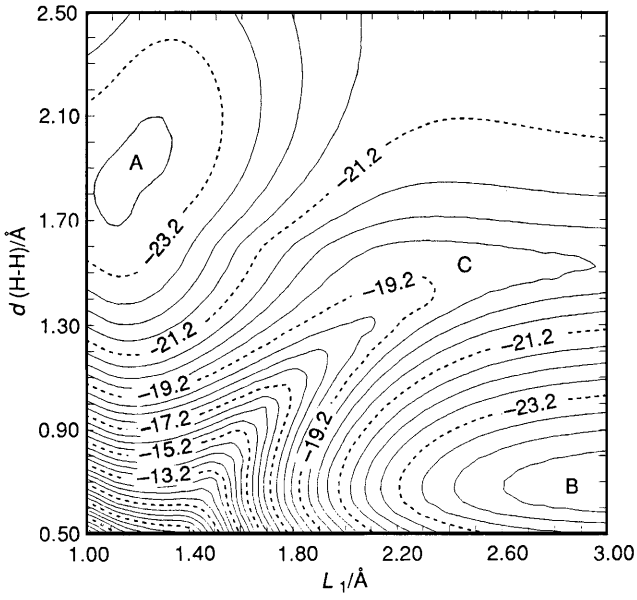

Fig. 16 Potential surface for the apical side-on interaction path **II**. Energies in eV. The energy separation of two contours is 0.5 eV

orbitals; see also Table 2. We therefore have to show only these orbitals in Fig. 15, where the lowest-lying A_1 has been dropped since it does not contribute significantly. The $3A_1$ and the $4A_1$ orbitals change very little along this path. They have to avoid crossing since C_{3v} symmetry is maintained. We can now see where the lowering of the energy barrier with respect to dissociation of H_2 comes from, as we proceed from E to D. Since the $A_1(\sigma_g)$ and $2A_1$ cannot cross, they mix in such a way that the former is stabilized and changes its shape, while $2A_1$ increases in energy and contributes the large part of the activation energy. This interaction can roughly be described as $2A_1 \pm A_1(\sigma_g)$ or in a more precise way as written in equation (23). The balance of stabilization and destabilization lowers the barrier by more than a factor of 2 with respect to the H–H bond energy.

Orbitals of A_1 and of E symmetry are involved in the apical side-on reaction, case **II** in Scheme 11. They can be written as in equations (24) and (25). The meaning of the formulae is

$$\Psi_{II\pi} = a_{II\pi}\sigma_u + \sum_{i=1}^{5} c^{E}_{IIj}(jE) \quad (24)$$

$$\Psi_{II\sigma} = a_{II\sigma}\sigma_u + \sum_{i=1}^{5} c^{A}_{IIi}(iA_1) \quad (25)$$

explained in Scheme 13. The x axis is parallel to σ_u which can interact with the E_x part of the two-fold degenerate E orbitals. If we now look at the potential-energy map in Fig. 16, we see that this interaction leads to the five-co-ordinate silicon intermediate

Published on 01 January 1991 on http://pubs.rsc.org | doi:10.1039/DT9910000917
Downloaded by Cornell University on 07 December 2012

View Article Online

Published on 01 January 1991 on http://pubs.rsc.org | doi:10.1039/DT9910000917
Downloaded by Cornell University on 07 December 2012

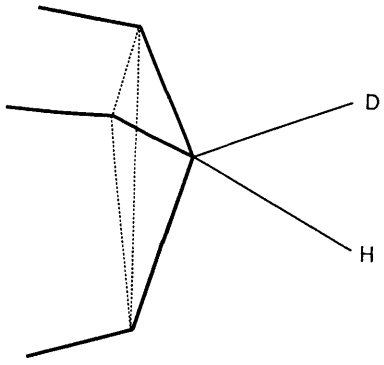

Scheme 14

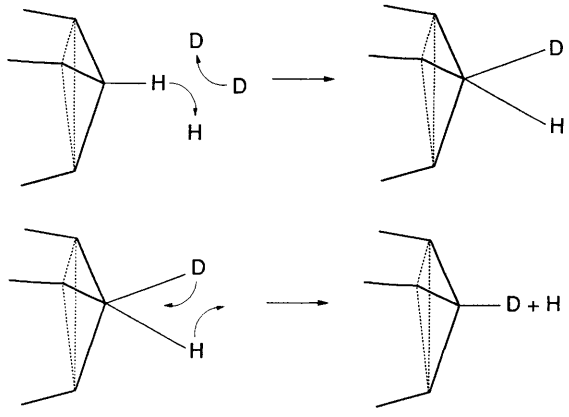

Scheme 15

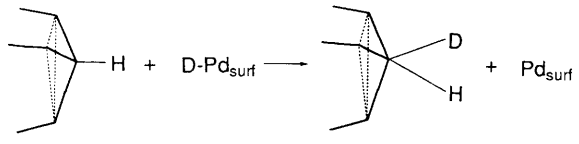

Scheme 16

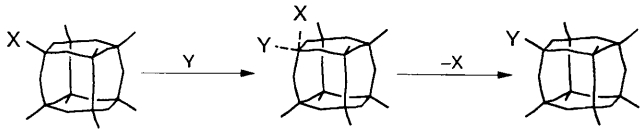

Scheme 17

in Scheme 14 with an H–Si–H angle of 120°. The proof that A is really a minimum comes from path **III** which is investigated below. The existence of such an intermediate is plausible and finds its counterpart in the chemistry of phosphorus compounds. With respect to the investigations of nucleophilic substitution reactions on four-co-ordinated Si by Holmes[1] and others,[2,6] this leads to a reaction mechanism which to our knowledge has not been proposed up to now. The reason for this lies in the rigidity and cage size of $H_8Si_8O_{12}$, which does not allow pseudo-rotation nor an attack from the back. Therefore a different mechanism for the rearrangement of the five-co-ordinated Si has to be advanced.

We propose that a probable reaction path for the deuterium-exchange reaction proceeds *via* five-co-ordinated Si (Scheme 14). Let us therefore study how such an intermediate can rearrange to form the desired product. In Fig. 17 we show the potential-energy map for reaction path **III** (Scheme 11). Starting at point A, it is obvious that the low-energy path proceeds *via* concerted decrease of the angles α_1 and α_2 and an increase of the L_1 distance, which results in an increase of the H–H separation and an approach *versus* the Si–H bond distance. This reaction path has a low activation energy.

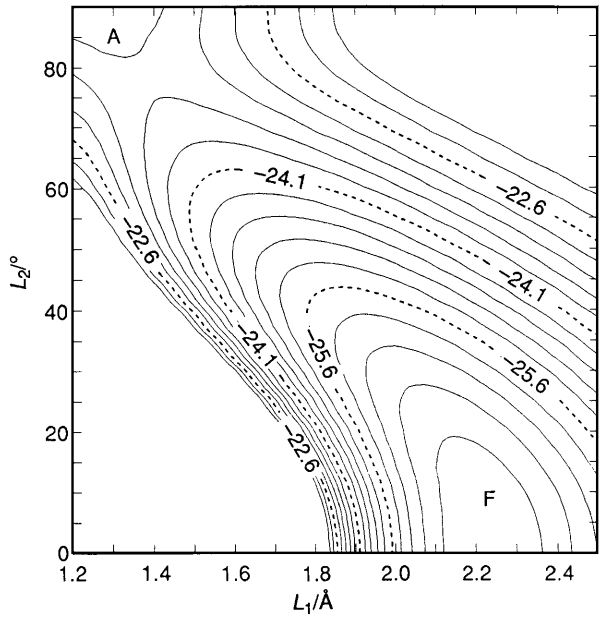

Fig. 17 Potential surface for interaction path **III**. Energies in eV. The coordinate L_2 can be written as $(\alpha_1^0 - \delta, \alpha_2^0 - \delta)$, where $\alpha_1^0 = \alpha_2^0 = 90°$. The energy separation of two contours is 0.3 eV

Summarizing these results leads to the conclusion that the reaction mechanism describing the deuterium exchange reaction (11) can be rationalized as shown in Schemes 15 and 16. The five-co-ordinate silicon intermediate is formed in a first step. There is an obvious similarity here to what is believed to happen in reactions catalysed on transition-metal surfaces.[28] Thus the mechanism of activation of D_2 is presumably that in Scheme 16, similar to Scheme 15. Once this intermediate has been formed, there is a 50% chance that O_3Si–D results. If D_2 is available in large excess over H_2 the deuterium exchange will be complete, as observed experimentally.[8]

If we now try to generalize these results, it seems very probable that all reactions in Scheme 2 proceed by the same mechanism, involving a five-co-ordinate silicon intermediate followed by the proposed rearrangements (Scheme 17). This can explain why no substitution of this type has been reported in alkyl and aryl $X_8Si_8O_{12}$ molecules. Too bulky substituents prevent the Si from building a five-co-ordinate intermediate. An attack from the back, as observed in many nucleophilic substitution reactions of Si, is not possible for steric reasons. An interesting example of such a reaction could be the addition of olefins Y to $H_8Si_8O_{12}$ in a hydrosilation reaction,[29] leading to the substitution of H by C and thus to the formation of an Si–C bond. Indeed the first reaction of this type has been successfully accomplished.[30]

Appendix

All calculations were carried out by the extended-Hückel method,[31] with the parameters collected in Table A1. Parameters were kept constant during all the calculations. Mulliken population analysis was applied[32] and the coulomb integrals H_{ii} in Table A1 were obtained by charge iteration on the corresponding $X_8Si_8O_{12}$ molecules at equilibrium geometry with the parameters from ref. 33. The off-diagonal elements were calculated as[34] in equation (A1). To approximate the

$$H_{ij} = \tfrac{1}{2}KS_{ij}(H_{ii} + H_{jj}) \qquad \text{(A1)}$$

Wolfsberg–Helmholz constant we used the weighted formula[35] (A2) in its distance-dependent form, as explained in a previous

View Article Online

Table A1 EHMO parameters; $k = 2.0$, $\delta = 0.35$

	N	n_s	ζ_s	H_{ss}/eV	n_p	ζ_p	H_{pp}/eV
Si	4	3	1.600	−20.44	3	1.600	−12.41
O	6	2	2.275	−26.13	2	2.275	−10.80
C	4	2	1.625	−19.54	2	1.625	−10.82
H	1	1	1.300	−13.43			
Cl	7	3	2.183	−19.54	3	1.733	−10.82

Table A2 Comparison of calculated and experimental bond lengths (Å)

Molecule	X	d(Si–X) exp.	d(Si–X) calc.
SiO		1.55	1.45
$Si(OH)_4$*		1.63–1.67	1.75
$X_8Si_8O_{12}$	H	1.45	1.23
	O	1.62	1.72
	CH_3	1.89	1.85
	Cl		1.80
$SiX(OH)_3$	H		1.23
	OH		1.75
	CH_3		1.84
	Cl		1.80

* d(O–H) = 0.947 (calc. 1.02) Å

$$K = 1 + \kappa e^{-\delta(R-d_0)} \qquad \text{(A2)}$$

paper.[22] A two-body term, as explained in refs. 21 and 22 has been added to correct for the core–core repulsion. Calculations including d orbitals on Si have shown that they can be neglected. To get an idea of the reliability of bond distances calculated in this paper, some data are collected in Table A2.

Acknowledgements

We would like to thank Professor R. Gleiter, University of Heidelberg, for measuring the photoelectron spectra of $H_8Si_8O_{12}$. G. C. also thanks Heribert Bürgy and Daniel Herren, University of Bern, for their contributions. This work is part of project NF 2-5.542 financed by the Schweizerischer Nationalfonds zur Förderung der wissenschaftlichen Forschung and by NEFF Project 329.

References

1 R. R. Holmes, *Chem. Rev.*, 1990, **90**, 17.
2 (*a*) R. Hoffmann, J. M. Howell and E. L. Muetterties, *J. Am. Chem. Soc.*, 1972, **94**, 3047; (*b*) R. R. Holmes, *J. Am. Chem. Soc.*, 1978, **100**, 433; (*c*) J. A. Deiters, R. R. Holmes and J. M. Holmes, *J. Am. Chem. Soc.*, 1988, **110**, 7672; (*d*) J. Woning, L. M. Daniels and J. G. Verkade, *J. Am. Chem. Soc.*, 1990, **112**, 4601.
3 V. W. Day, W. G. Klemperer, V. V. Mainz and D. M. Millar, *J. Am. Chem. Soc.*, 1985, **107**, 8262.
4 D. W. Scott, *J. Am. Chem. Soc.*, 1946, **68**, 356; A. J. Barry, W. H. Daudt, J. J. Domicone and J. W. Gilkey, *J. Am. Chem. Soc.*, 1955, **77**, 4248; R. Müller, R. Köhne and S. Sliwinski, *J. Prakt. Chem.*, 1959, **9**, 71.
5 K. Larsson, *Ark. Kemi*, 1960, **16**, 215.
6 (*a*) L. H. Vogt, jun. and J. F. Brown, jun., *Inorg. Chem.*, 1963, **2**, 189; (*b*) J. F. Brown, jun., L. H. Vogt, jun. and P. I. Prescott, *J. Am. Chem. Soc.*, 1964, **86**, 1120; (*c*) C. L. Frye and W. T. Collins, *J. Am. Chem. Soc.*, 1970, **92**, 5586; (*d*) for a recent review, see E. Lukevics, O. Pudova and R. Sturkovich, *Molecular Structure of Organosilicon Compounds*, Ellis Horwood, Chichester, 1989; (*e*) F. J. Feher and Th. A. Budzichowski, *J. Organomet. Chem.*, 1989, **373**, 153; **379**, 33; (*f*) H. Bürgy, G. Calzaferri, D. Herren and A. Zholanov, *Chimia*, 1991, **45**, 3.
7 P. A. Agaskar, V. W. Day and W. G. Klemperer, *J. Am. Chem. Soc.*, 1987, **109**, 5554.
8 H. Bürgy and G. Calzaferri, *Helv. Chim. Acta*, 1990, **73**, 698.
9 P. Bornhauser and G. Calzaferri, *Spectrochim. Acta, Part A*, 1990, **46**, 1045.
10 R. Beer, H. Bürgy, G. Calzaferri and I. Kamber, *J. Electron Spectrosc. Relat. Phenom.*, 1987, **44**, 121.
11 (*a*) J. W. Ward and R. C. Hansford, *J. Catal.*, 1969, **13**, 364; (*b*) D. W. Breck, *Zeolite Molecular Sieves*, Wiley, New York, 1974; (*c*) J. M. Thomas, *Angew. Chem., Int. Ed. Engl.*, 1988, **27**, 1673; (*d*) J. Baumann, R. Beer, G. Calzaferri and B. Waldeck, *J. Phys. Chem.*, 1989, **93**, 2292; (*e*) G. A. Ozin and J. Godber, *J. Phys. Chem.*, 1989, **93**, 878; (*f*) J. Sauer, *Chem. Rev.*, 1989, **89**, 199.
12 G. Calzaferri and L. Forss, *Helv. Chim. Acta*, 1987, **70**, 465; 1986, **69**, 873.
13 D. L. Griscom, *J. Non-Cryst. Solids*, 1977, **24**, 155.
14 W. M. Meier and D. H. Olson, *Atlas of Zeolite Structure Types*, 2nd edn., Butterworth, London, 1988.
15 R. Ahlrichs, M. Bär, M. Häser, Ch. Kölmel and J. Sauer, *Chem. Phys. Lett.*, 1989, **164**, 199; J. Sauer, C. M. Kölmel, J.-R. Hill and R. Ahlrichs, *Chem. Phys. Lett.*, 1989, **164**, 193; L. N. Mazalov, S. A. Krupoder, A. V. Okotrub, V. V. Murakhtanov, I. P. Asanov, V. S. Danilovich, V. D. Yumatov, S. V. Basenko, R. G. Mirskov and M. G. Voronkov, *Dokl. Phys. Chem. Proc. Acad. Sci.*, 1988, **302**, 894.
16 T. P. E. Auf der Heyde, H. B. Bürgi, H. Bürgy, K. W. Törnroos, *Chimia*, **45**, in the press.
17 R. S. Mulliken, *J. Chem. Phys.*, 1933, **1**, 492; F. A. Cotton, *Chemical Application of Group Theory*, 2nd edn., Wiley, New York, 1971.
18 L. Salem, *Electrons in Chemical Reactions: First Principles*, Wiley, New York, 1982; T. A. Albright, J. K. Burdett and M.-H. Whangbo, *Orbital Interactions in Chemistry*, Wiley, New York, 1985.
19 T. Koopmans, *Physica*, 1934, **1**, 104.
20 D. W. Turner, C. Baker, A. D. Baker and C. R. Brundle, *Molecular Photoelectron Spectroscopy*, Wiley-Interscience, London, 1970.
21 A. B. Anderson and R. Hoffmann, *J. Chem. Phys.*, 1974, **60**, 4271.
22 G. Calzaferri, L. Forss and I. Kamber, *J. Phys. Chem.*, 1989, **93**, 5366.
23 R. D. Levine and R. B. Bernstein, *Molecular Dynamics and Chemical Reactivity*, Oxford University Press, Oxford, 1987, ch. 4; K. J. Laidler, *Chemical Kinetics*, McGraw-Hill, New York, 1950.
24 R. S. Mulliken, *J. Chem. Phys.*, 1939, **7**, 339.
25 M. J. S. Dewar, *Hyperconjugation*, Ronald Press, New York, 1962; R. Hoffmann, L. Radom, J. A. Pople, P. R. Schleyer, W. J. Hehre and L. Salem, *J. Am. Chem. Soc.*, 1972, **94**, 6221; P. D. Mollère and R. Hoffmann, *J. Am. Chem. Soc.*, 1975, **97**, 3680; R. Hoffmann and P. Hofmann, *J. Am. Chem. Soc.*, 1976, **98**, 598.
26 R. Gleiter and G. Calzaferri, unpublished work.
27 H. Bock, *Angew. Chem.*, 1989, **101**, 1659.
28 J.-Y. Saillard and R. Hoffmann, *J. Am. Chem. Soc.*, 1984, **106**, 2006.
29 J. W. Wilt, *Reaction Intermediates*, ed. R. A. Abramovich, Plenum, New York, 1983, vol. 3, p. 113.
30 D. Herren, H. Bürgy and G. Calzaferri, *Helv. Chim. Acta*, 1991, **74**, 24.
31 R. Hoffmann, *J. Chem. Phys.*, 1963, **39**, 1397.
32 R. S. Mulliken, *J. Chem. Phys.*, 1955, **23**, 1833.
33 H. Basch, A. Viste and H. B. Gray, *Theor. Chim. Acta*, 1965, **3**, 458.
34 M. Wolfsberg and L. Helmholz, *J. Chem. Phys.*, 1952, **20**, 837.
35 J. H. Ammeter, H.-B. Bürgi, J. C. Thibeault and R. Hoffmann, *J. Am. Chem. Soc.*, 1978, **100**, 3686.

Received 2nd *July* 1990; *Paper* 0/02970J

Published on 01 January 1991 on http://pubs.rsc.org | doi:10.1039/DT9910000917
Downloaded by Cornell University on 07 December 2012